PAPER

CrossMark
click for updates

UV-assisted synthesis of indium nitride nano and microstructures†

Mahalieo Kao,[ab] Rudolph M. Erasmus,[bd] Nosipho Moloto,[a] Neil J. Coville*[ab] and Sabelo D. Mhlanga*[bc]

Indium nitride (InN) has been made the first time by a combined thermal/UV photo-assisted process. Indium oxide (In_2O_3) was reacted with ammonia using two different procedures in which either the ammonia was photolysed or both In_2O_3 and ammonia were photolysed. A wide range of InN structures were made by these procedures that were determined by the reaction conditions (time, temperature). The reaction of In_2O_3 with photolysed NH_3 gave InN rod-like structures that were made of stacked cones (6 h/750 °C) or discs (6 h/800 °C) and that contained some In_2O_3 residue. In contrast, photolysis of both In_2O_3 and NH_3 gave InN nanowires and pure InN nanotubes filled with In metal (>90%). The transformation of the 3D In_2O_3 particles to the tubular 1D InN was monitored as a function of time (1–4 h) and temperature (700–800 °C); the product formed was very sensitive to temperature. The band gap of the In filled InN nanotubes was found to be 1.89 eV.

1 Introduction

InN is an understudied material because it is difficult to produce due to its low decomposition temperature and its high equilibrium pressure with N_2.[1] This has led to many controversies about the properties of this material. The inconsistencies and lack of reproducibility observed in the reported syntheses for this material escalates the problem.

InN has been grown with morphologies that range from one dimension (1D) to three dimensions (3D).[2,3] 1D nanostructures are of particular importance in nanoscience and nanotechnology since they can be used to control space-confined transport phenomena,[4,5] exhibit a discrete density of states and at the same time maintain a continuous transport path.[6] They are of great importance in the understanding of the fundamental properties of low dimensional systems, and for use in potential nanodevice applications.[7]

Chemical vapour deposition (CVD) has proven to be a feasible method to prepare 1D InN nanomaterials.[8–11]

ᵃMolecular Sciences Institute, School of Chemistry, University of the Witwatersrand, Johannesburg 2050, South Africa. E-mail: Neil.coville@wits.ac.za

ᵇDST-NRF Centre of Excellence in Strong Materials, University of the Witwatersrand, Johannesburg 2050, South Africa

ᶜNanotechnology and Water Sustainability Research Unit, College of Science, Engineering and Technology, University of South Africa, Florida Science Campus, Johannesburg, South Africa. E-mail: mhlansd@unisa.ac.za

ᵈRaman and Luminescence Laboratory, School of Physics, University of the Witwatersrand, Johannesburg 2050, South Africa

† Electronic supplementary information (ESI) available: XRD patterns of InN materials with oxide impurities synthesised from a reaction of In_2O_3 with photolysed NH_3 at different temperatures for a period of 6 h. See DOI: 10.1039/c4ta06848c

Temperature has been identified as a driving force that determines the different types of morphologies of the 1D InN nanostructures synthesised by CVD.[11–13] The many studies reported on the synthesis of 1D InN using CVD have related to InN nanowires while much less work has been done on the synthesis of InN nanotubes.[7,10–12,14]

In_2O_3 is very attractive as an indium source in CVD studies due to the ease with which it can be handled. Body centred cubic In_2O_3 with space group *Ia*3 has a direct band gap and dominant ionic bonding.[15] The magnitudes of the absorption and reflection coefficients for In_2O_3 are low, in the energy range 0–5 eV, indicating transparency in the material.[15] It has a band gap of 3.6 eV.[16]

Several CVD studies have reported on the use of In_2O_3 for the preparation of InN. Zhang *et al.* reported the synthesis of InN nanowires through nitridation of a mixture of In metal and In_2O_3 (mole ratio 4 : 1) at 700 °C for a reaction time of 4 h in NH_3.[8] However the XRD pattern of the InN showed the existence of an oxide impurity. On the other hand Tang *et al.* have reported the preparation of single crystal InN nanowires by nitriding a mixture of In metal and In_2O_3 (mole ratio ~5 : 1) at 525 °C for a period of 30 min under NH_3, based on a SAED pattern of a hexagonal crystal system and Raman spectroscopy.[9] At the other extreme, carbonitridation of In_2O_3 *via* CVD for 1.5 h was reported to give InN nanowires at 1150–1180 °C and InN nanotubes at 1190–1220 °C.[14] Gao *et al.* reported complete nitridation of nanosized In_2O_3 and $In(OH)_3$ powders within 8 h at 600 °C under NH_3.[17] In contrast, Luo *et al.* have reported several studies on the synthesis of InN and reported complete conversion of In_2O_3 powder to InN nanowires at 700 °C for a reaction period of 8 h in NH_3 whereas for a shorter time period

(4 h) oxide impurities were noted in their study.[18] In a related study, done by a different group, a change in dimensionality on nitridation of In$_2$O$_3$ (650–700 °C for 4 h), was reported.[11] Dimensional and structural evolution from 1D InN nanowires to 2D InN plates was achieved through temperature increments of 25 °C.[11] Luo *et al.* also reported on the impact of reaction time on the morphologies of structures resulting from nitridation of In$_2$O$_3$ at 680 °C in the presence of a gold catalyst. In this study, both InN nanowires (14 h) and InN nanobelts (38 h) were produced.[19] In yet another study at, 680 °C, Luo *et al.* made pure InN nanobelts (22 h); microtubes coexisting with nanobelts after 26 h, but after 30 h microtubes dominated.[10] It has also been reported that a dramatic change in InN morphology with temperature indicated predominant involvement of In$_2$O gas, formed from the decomposition of In$_2$O$_3$, in the growth of InN structures.[12]

It can be seen from the studies mentioned that the standard reaction parameters for the synthesis of InN tubes from In$_2$O$_3$ have not yet been confirmed and agreed upon. The reported reaction parameters show wide ranges involving a single parameter such as the type of nitrogen source (N$_2$, NH$_3$), the flow rate (30–500 sccm), the time of reaction (1½–30 h) and the temperature (680–1220 °C).[7,10–12,14] More than two thirds of the reported InN tubes are in the micrometer scale and the longest InN tubes reported are several microns in length.[7]

This study reports on the first UV photochemical synthesis of a range of InN structures as well as partially filled indium nitride nanotubes by photo-assisted nitridation of In$_2$O$_3$ in NH$_3$. Photo-assisted reactions are typically done with lasers due to their high peak intensities.[20] However, UV-photochemical vapour deposition (UV-CVD) has been successfully used in the past to deposit numerous metals, insulators, and semiconducting films.[21–23] In photochemical reactions, absorption of light by a reactant molecule enables an inaccessible reaction path to occur by bringing the reactants to the necessary activation energy and also by changing the symmetry of the reactant's electronic configuration.[24] Medium pressure mercury UV lamps are important radiation sources for photochemical applications. When medium pressure mercury lamps are used more energy levels are excited resulting in more spectral lines as well as a continuum due to recombination radiation.[25] The major UV spectral lines emitted by these lamps are at 254 nm (4.8 eV) and 185 nm (6.7 eV). The majority of the UV-photochemical studies reported to date has focused on the deposition of two dimensional (2D) structures (*i.e.* thin films).[26] Most films are normally produced using plasma deposition techniques in glow discharge.

UV-photochemical deposition of 1D group III-nitride nanostructures, with NH$_3$, is not well established. Boron nitride nanotubes were synthesized by using excimer laser ablation at 1200 °C in different carrier gases.[27] A few UV-synthesis studies have been reported on 1D gallium nitride (GaN) nanostructures. Shi *et al.* reported on GaN nanowires made from gallium oxide, using an excimer pulsed laser.[28] Lieber and Duan also synthesised GaN nanowires by laser ablation of a metal containing target.[29] There are however, to our knowledge, no studies reported on UV-CVD synthesis of one dimensional (1D) III-nitrides in general, and specifically on indium nitride (InN).

2 Results and discussion

2.1 InN synthesis by photolysis of only NH$_3$

The effect of photo-activating only the ammonia in the nitridation of In$_2$O$_3$, was investigated by placing a boat containing In$_2$O$_3$ downstream out of the UV-light (*i.e.* the sample was protected from the UV light) (Fig. 1, position 1). In the absence of photolysis and using this configuration, ($T > 700$ °C) no InN was formed. Also, photolysis performed below 700 °C, yielded no InN. This is to be contrasted with reports on the production of InN at much lower temperatures using plasma assisted CVD.[30]

Reactions involving the photolysis of NH$_3$ in position 1 (Fig. 1) were also performed for 6 h at 700, 750 and 800 °C and soft black powders or dark brown fluffy materials were produced and collected from the quartz boat. In reactions performed for shorter times, the product was dominated by In$_2$O$_3$ (see Table S1†).

The XRD patterns of the as-synthesised materials made at 700–800 °C (Fig. S1†) revealed that after 6 h wurtzite InN was formed in all reactions but the product contained varying amounts of In$_2$O$_3$. XRD analysis showed that In$_2$O$_3$ in the product did not decrease substantially with increasing temperature as one might expect. Microscopy analysis also revealed that the indium oxide signals found in the InN XRD pattern are due to large residual In$_2$O$_3$ particles which did not completely react; the residual In$_2$O$_3$ was not due to a residual oxide coating of the InN. For materials made at 800 °C after 6 h reaction, spherical droplets of metallic indium were also observed at the bottom of the quartz boat. The images shown in Fig. 2 correspond to InN structures and indicate the variability in InN morphologies formed by variation in temperature.

TEM and SEM images of the precursor In$_2$O$_3$ prior to reaction showed solid agglomerated well defined 3D facetted particles with varying dimensions (Fig. 2a and b). Higher magnification SEM images reveal that all the particle tips sticking out from the agglomerate have rhombohedral-like faces varying in size that depend on both the size of the parent particle and the extent it is embedded into the agglomerate (Fig. 2b insert). TEM and SEM analyses of the collected materials after 6 h at 700 °C showed that the product consisted of an
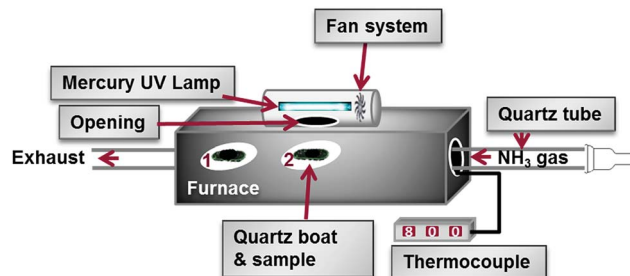

Fig. 1 A horizontal CVD furnace with a mercury UV lamp housing equipped with a cooling fan system. Position 1 is the position where NH$_3$ was irradiated but the quartz boat and its contents were not irradiated by UV-light. Position 2 marks the position where the NH$_3$, the quartz boat and its contents are illuminated by the UV-light.
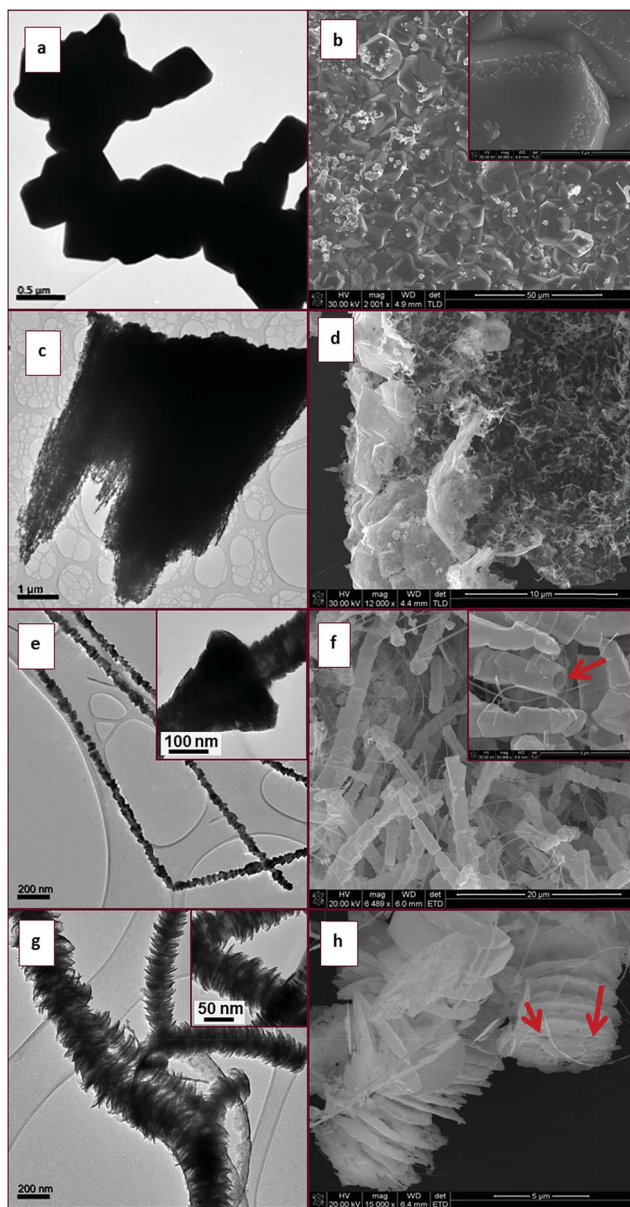
Fig. 2 (a) TEM and (b) SEM images of as purchased In_2O_3 particles, (c) TEM and (d) SEM images of perforated materials formed at 700 °C, (e) TEM and (f) SEM images of segmented rod like structures at 750 °C (the arrow indicates the hollow core), (g) TEM and (h) SEM images of flaky structures at 800 °C (the arrows show perforations). All reactions were performed by photolysis of NH_3 only.

irregularly perforated material (Fig. 2c and d). At 750 °C TEM and SEM images revealed that rod-like structures had formed (Fig. 2e and f). These rod-like structures possessed rough surfaces (Fig. 2e). High magnification TEM analysis of the rod-like structures showed that the roughness is due to stacking of cone like pieces that form the overall structure (Fig. 2e insert). An arrow shows that some of the cones are actually hollow, an indication that the rod-like structures are tubular in nature (Fig. 2f insert).

At 800 °C SEM analysis revealed that unusual 1D structures were formed from stacked disc-like units (Fig. 2h). The flake-

like nature of the stacked discs creates an illusion of a rod-like structure, as revealed by the high magnification TEM image (Fig. 2g insert). The flakes had a rough surface texture and arrows indicate some of the perforations on the surface of the flakes (Fig. 2h). This disc type of morphology has not been reported previously in the literature for InN nanostructures.

In summary, even though a 100% pure InN material was not synthesized from photolysis of only NH_3, information on the structure generation as a function of temperature was obtained. We suggest that the In_2O_3 was etched by the species generated by photolysis of NH_3 in the process of nitridation (in the absence of photolysis no InN was made under the reaction conditions studied). No oxide nanowires were observed but the parent oxide particles were observed. The species formed from NH_3 degrade the oxide leading to formation of InN with a disc like appearance and with increased temperature these discs become longer and more flake like.

2.2 InN synthesis by photolysis of both indium oxide and NH_3

2.2.1 XRD studies. In an attempt to obtain pure InN, In_2O_3 and NH_3 were both irradiated with UV-light at different temperatures (700–800 °C) for a maximum period of 2 h to minimise concurrent photodecomposition of the product (Table S1†). XRD patterns obtained from the as-synthesised material prepared at different temperatures showed enhanced improvement in InN purity with increasing temperature (Fig. 3). The (101) peak intensity of the cubic In_2O_3 reactant (seen at $35.8°\theta$) decreased gradually with increasing temperature until it was hardly observable at 800 °C; inversely the InN (002) peak intensity at $36.6°\theta$ became prominent with temperature (Fig. 3). Thus, photoactivation of both In_2O_3 and NH_3 improved the chemical purity of the InN product. Total conversion of In_2O_3 to InN was however not attained in 2 h in the temperature range studied.
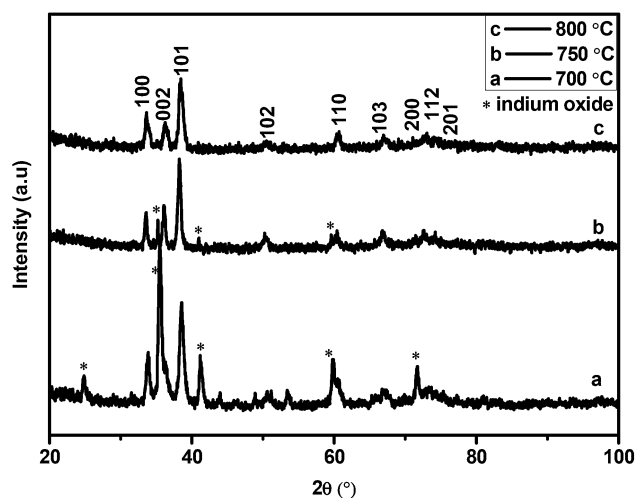

Fig. 3 XRD patterns of wurtzite InN materials prepared from photolysis of In_2O_3 and NH_3 in 2 h at different temperatures.

5964 | J. Mater. Chem. A, 2015, 3, 5962–5970

This journal is © The Royal Society of Chemistry 2015

2.2.2 Microscopy studies. TEM and SEM analyses of the product formed at different temperatures were studied and the images revealed that there is a gradual change from In_2O_3 3D microparticles to 3D InN microstructures at 700 °C (Fig. 4a and b); and finally to 1D InN nanostructures at 800 °C (Fig. 4e and f). A change from microparticles to nanotubes with temperature had occurred. At 700 °C porous particles dominate (Fig. 4a and b). At 750 °C few particles and microsheets coexist with amorphous nanowires (Fig. 4c and d). It can be seen from the TEM image that some nanowires show *Y*-junction features (Fig. 4c insert). At 800 °C TEM and SEM analyses revealed InN nanotubes (diameter ~40 nm) as the dominant species (Fig. 4e and f).

2.3 Photolysis of indium oxide and NH₃ as a function of time

2.3.1 XRD studies. XRD analysis of the materials made in 2 h at 750 °C and 800 °C indicated the presence of minute residual oxide impurities as compared to materials made at 700 °C (Fig. 3). The impact of time on the InN materials was therefore investigated at 750 °C and 800 °C. Reactions were performed at both temperatures in the time range of 30 min to

Fig. 5 XRD patterns of wurtzite InN materials prepared at 750 °C for different duration.

4 h. Microscopy analysis of materials collected from times shorter than 2 h also provided information on the mechanism of conversion from 3D In_2O_3 microstructures to 1D InN nanostructures. XRD analysis of materials made at 750 and 800 °C, showed gradual improvement in chemical purity (Fig. 5 and 6). The XRD patterns collected from the product obtained after reaction times of 3–4 h indicated complete conversion of the oxide to indium nitride (Fig. 5 and 6). However, the production of pure InN using longer reaction times, under UV irradiation, also gave metallic indium droplets that were detected at the base of the quartz boat. This reduced the yield of the final InN product.

2.3.2 Microscopy analysis of InN nanowires at 750 °C as a function of time. Nanowires were observed for all reactions performed at 750 °C. The nanowires varied in abundance, length and crystallinity with time. The TEM and SEM images showed that nitriding In_2O_3 at 750 °C for 30 min largely resulted
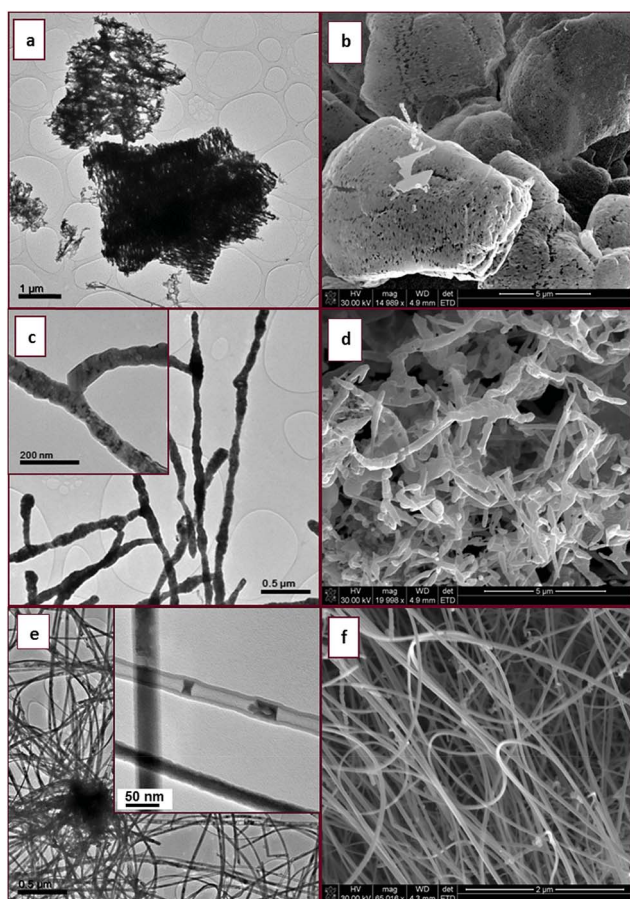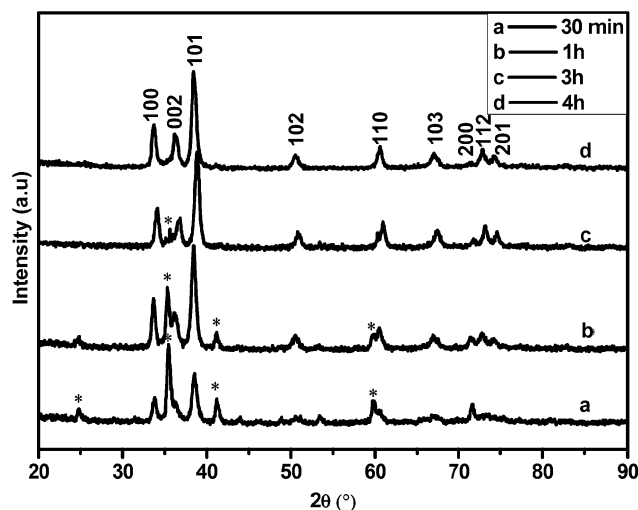

Fig. 4 (a) TEM and (b) SEM images of porous InN particles showing irregular pores at 700 °C, (c) TEM and (d) SEM images of amorphous nanowires at 750 °C, (e) TEM and (f) SEM images of partially filled InN tubes at 800 °C. All reactions were held for 2 h at their respective temperatures.
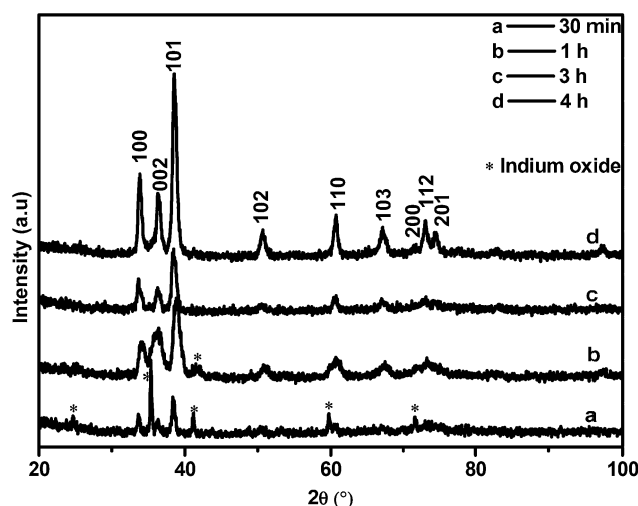

Fig. 6 XRD patterns of the wurtzite InN product synthesised by photoactivation of In_2O_3 and NH₃ at 800 °C as a function of time.
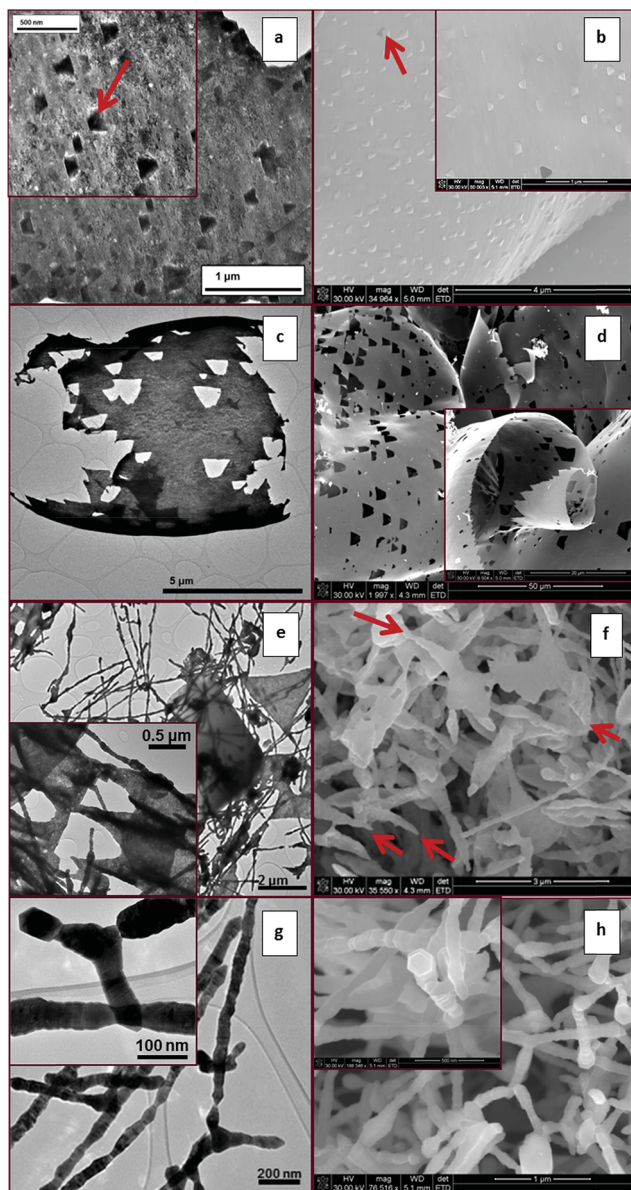
Fig. 7 (a) TEM and (b) SEM images of 2D microsheets at 750 °C for 30 min; (c) TEM and (d) SEM images of perforated 2D microsheets at 750 °C for 1 h; (e) TEM and (f) SEM images of amorphous InN nanowires formed from 2D microsheets at 750 °C for 2 h; (g) TEM and (h) SEM images of InN nanowires at 750 °C for 3–4 h.

2.3.3 Microscopy analysis of InN nanotubes at 800 °C as a function of time. Interestingly, the structures obtained from nitriding 3D In_2O_3 particles at 800 °C deviate completely from those obtained at 750 °C indicating that the mechanism of formation is temperature dependent. The sample made in 30 min at 800 °C consisted largely of the In_2O_3 particles with only a few tubes (Fig. 8a and b) and this finding is consistent with XRD data. After 1 h the material contained a small fraction of remnants of In_2O_3 particles but InN nanotubes now dominated the mixture (Fig. 8c and d). An impressive improvement in selectivity of tubes over other structures is seen after 2–3 h (Fig. 8e and f). Finally complete conversion to InN nanotubes is noted after 4 h (Fig. 8g and h). High magnification TEM analysis
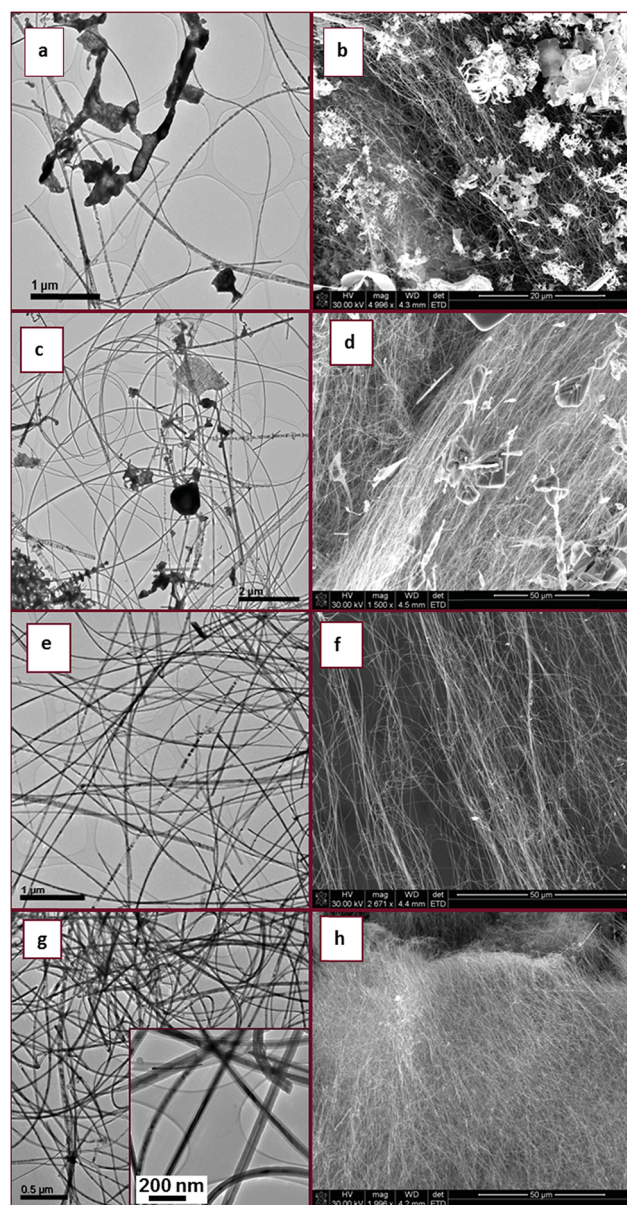
Fig. 8 (a) TEM and (b) SEM images of InN nanotubes at 800 °C in 30 min. (c) TEM and (d) SEM images of the nanotubes at 800 °C for 1 h (e) TEM and (f) SEM images of the nanotubes at 800 °C for 3 h, (g) TEM and (h) SEM images of the nanotubes at 800 °C for 4 h.

in the formation of 2D microsheets. The TEM and SEM images of the 2D microsheets showed rhombohedral particles embedded into the matrix of the 2D microsheet and thus created mounds (Fig. 7a and b). A high magnification TEM image of the sheet showed that the edges around the rhombohedral particles were slightly perforated and created crevices (Fig. 7a insert). These crevices are points of weakness on the 2D sheet. The TEM and SEM images showed the rhombohedral particles on the 2D sheet indicated by arrows (Fig. 7a and b). Nitriding for 1 h at 750 °C resulted information of porous 2D microsheets with rhombohedral holes of varying sizes due to loss of the rhombohedral particles originally embedded in the 2D structure.

revealed that the nanotubes are partially filled with indium (Fig. 8g insert). Approximately 90% of the InN nanotubes made in this study are partially filled with indium. The indium filled nanotubes have a core–shell structure appearance (Fig. 8g insert). TEM analysis revealed that approximately 60% of the InN nanotubes have diameters around 30–40 nm (Fig. 9), and are a few hundred microns in length (Fig. 8h).

To our knowledge indium filled InN nanotubes have not been previously reported. However, GaN nanotubes partially filled with indium have been achieved through indium assisted thermal evaporation. It was suggested that indium played an important role in the formation of nanotubes since spherical indium particles were found at the tips of the GaN tubes.[31] We propose that InN nanotubes may develop from both 2D sheets and 3D microparticles as long as the reaction conditions generate an indium catalyst essential for tube formation. In our study the general quality and selectivity of the product (InN) improved gradually with increasing time of reaction.

2.4 Spectral properties of In filled InN nanotubes

Fig. 10 shows the Raman spectrum of the partially filled InN nanotubes made at 800 °C (2 h). The E_2 high mode of the wurtzite InN is observed at 478 cm^{-1}. The strain-free Raman frequency of the E_2 high mode has been reported to be 490 cm^{-1} for wurtzite InN.[32] Hence it is blue shifted relative to the reported position for strain free InN. Usually a shift to lower wavenumbers indicates the presence of tensile stress. The Raman peak at 581 cm^{-1} is also blue shifted ($\sim$4 cm^{-1}) relative to the A_1 longitudinal optical (LO) mode reported at 585–590 cm^{-1}.[33] The data thus indicates tensile stress in the material.

The fundamental band gap value for InN is still a subject of controversy. The values from the reported data vary between 0.65 eV to 2.1 eV.[34] Various phenomena, mechanisms and processes such as deep level traps, the Mie resonance, the Burstein–Moss effect, quantum confinement, oxygen incorporation and nitrogen-vacancies have been proposed to explain the band gap values measured for InN.[34] It has also been shown
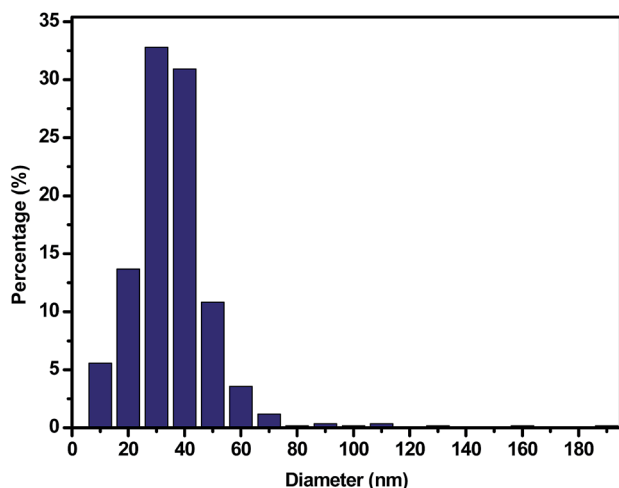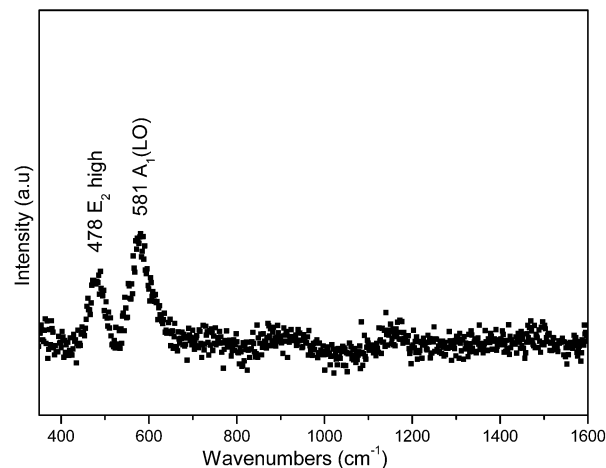

Fig. 10 Raman spectrum of partially filled InN nanotubes made at 800 °C.

that deviations in the In:N stoichiometric ratio can result in a large change in the band gap.[35] Polycrystallinity has been identified as one of the factors that may lead to high band gap values. In InN materials polycrystallinity has been associated with excess nitrogen; and it has been suggested that excess nitrogen incorporation occurs largely when non-equilibrium growth techniques such as RF sputtering, and MBE are used.[36]

UV-vis/NIR diffuse reflectance spectroscopy was used in this study to determine the band gap value of the partially filled InN nanotubes made at 800 °C for 4 h. It has been suggested that the DRS technique can allow for the extraction of the band gap values of powder semiconductors without any ambiguity.[37] The estimated band gap energy of partially filled tubes made at 800 °C was found to be 1.89 eV (Fig. 11 insert). This value is close to the original band gap data reported for InN (1.9 eV)[38] but much larger than the more recent band gap values reported (0.7 eV) for InN.[39] The observed band gap values might be influenced by the possible presence of defects suggested by

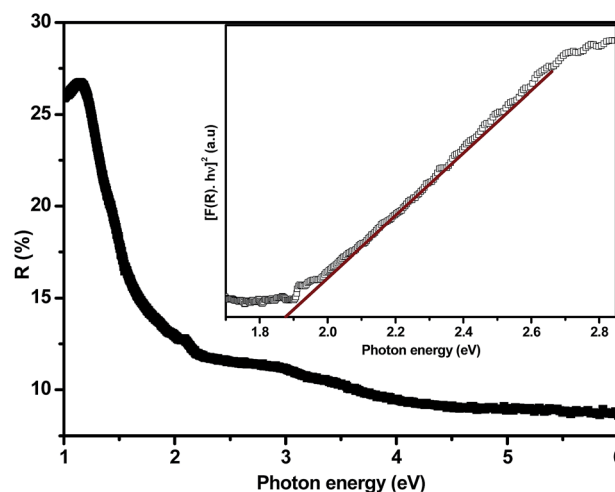Fig. 9 InN nanotube diameters obtained from TEM studies.

Fig. 11 Diffuse reflectance spectra of partially filled InN nanotubes at 800 °C. The insert shows the Kubelka–Munk function analyses of the DRS of partially filled InN tubes at 800 °C.

tensile stress indicated by Raman analysis. It also might to some extent be influenced by the indium within the core of the nanotubes.[34] The indium could increase the overall carrier concentration of the InN nanotubes. Large carrier concentrations have been correlated to high band gap values associated with the Burstein–Moss effect.[40]

2.5 Reaction mechanism

It is interesting to note that the morphologies of the synthesized 1D InN nanostructures depend remarkably on small changes in the growth temperature. Ding *et al.* reported that in the vapour–liquid–solid (VLS) mechanism the shape of a 1D structure is determined by the interfacial lattice mismatch between a catalyst particle and a 1D structure.[41] They however suggested that amongst other factors, temperature played a crucial role in determining the shape of a 1D structure but a detailed mechanism was not provided. Bando *et al.* and others suggested that in a vapour–solid (VS) mechanism, hollow InN nanotubes were formed by a diffusion-limited process at high temperatures, while the solid InN nanowires were formed by a kinetically limited process at lower temperatures in a VS mechanism.[14,42,43]

The InN obtained from the reaction between In_2O_3 and NH_3 generated by photo-activation of only NH_3, showed a change in the morphology with time and temperature. All samples contained small amounts of In_2O_3. The photo-activated reaction of both In_2O_3 and NH_3, as a function of temperature also gave rise to different morphologies of pure InN.

For all reactions in which only NH_3 was photolysed, a minimum of 6 h appears necessary to obtain InN even though it was still impure. The morphologies varied with temperature indicating that the mechanism of formation is temperature dependent.

The TEM and SEM analyses shed some light into the progressive development of 1D morphologies of InN from 3D In_2O_3 particles. It is suspected that the porous particles form from the solid In_2O_3 particles by thermal decomposition in a manner similar to that proposed by Yu *et al.*[44–46] This entails adsorption, diffusion and subsequent reaction of NH_3 species on and within the In_2O_3 particle core. A InN shell would be formed from surface based reactions on the outside the In_2O_3 core, later converting to a porous hollow particle (Fig. S2†). The general reaction between In_2O_3 and NH_3 proposed by several authors can explain the generation of H_2O as a by-product.[12,17,18,47] As decomposition of the In_2O_3 core proceeds in the presence of NH_3, the generated H_2O vapour accumulates in the core until the pressure, when high enough, weakens the shell of the particle generating tiny pores that allow the trapped gas to escape. Alternatively the pores could be formed by conversion of In_2O_3 to InN by NH_3; in the process the structure changes, as N replaces O. This is to be contrasted with the mechanism proposed by Ashok and co-workers to interpret the synthesis of porous InN microcages. Ashok *et al.* observed porous microcages in the InN synthesis using a lower temperature (650 °C) and a shorter reaction time (1 h). They suggested that microcages form by self-assembly of a few web-like structures controlled by a diffusion limited process.[48] In another study InN microtubes with holes

were observed and it was suggested that the holes were formed as a result of a lack of InN vapour in the reaction feed.[12]

The kinetics and the reaction mechanism for the photochemical decomposition of ammonia by ultraviolet light has not yet been settled,[49–51] and even in the simplest case of thermal NH_3 decomposition several matters are still in dispute.[52–54] However, both thermal and photochemical decomposition studies of NH_3 have identified N_2H_4 as the molecular intermediate formed before conversion to H_2 and N_2 (molar ratio 3 : 1).[50,52] NH_3 and N_2H_4 are known for their etching properties. We therefore propose that the 2D microsheets observed in this study are formed from surface etching of the 3D In_2O_3 particle agglomerates by UV-light, NH_3 and N_2H_4. Based on differences in the parent particle size as well as differences in exposure of the individual particles in the agglomerate, to the etching agents, some particles are selectively etched faster than others creating the 2D sheet with uneven points. As a result the particles least affected by etching remain stuck in the sheet creating mounds. Prolonged etching of the sheet creates weak points around the particles stuck in the parent sheet and the particles fall off the 2D sheet leaving behind rhombohedral holes on the 2D sheet. This is to be contrasted with the proposition made by Schwenzer *et al.*[11] They suggested that 2D microplates were formed by degradation of the InN microtube walls. They also observed triangular shaped holes on the microtubes. Our study helps bring into focus the mechanism of formation for the triangular/rhombohedral shaped holes observed on the InN microtubes/sheets.

Further degradation of the porous 2D sheet results in selective growth of the InN nanowires from the corners of the pieces of the parent sheet in a manner similar to that described by Schwenzer *et al.*[11] They observed that the corners of the triangles of 2D InN plates grow into nanowires. They suggested that the co-existence of nano and microstructures indicated that the structures do not form independently from In_2O_3 but rather go through different stages.[11] It is to be noted that another research study argued that the local differences in the morphology of InN structures suggested the independent growth of InN nano and microstructures.[12] The schematic presentation of our proposed mechanism for 1D InN growth is presented in Fig. 12. The mechanism of nanowire growth from 2D sheets is to be contrasted with the mechanism of nanowire growth from microcages proposed by Ashok *et al.*[48]
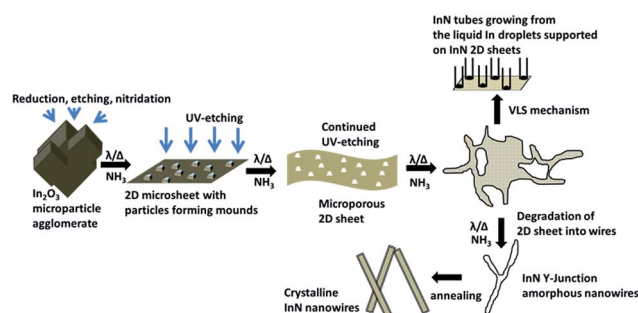

Fig. 12 Reaction mechanism showing etching effects due to both the UV and ammonia species.

5968 | *J. Mater. Chem. A*, 2015, **3**, 5962–5970

This journal is © The Royal Society of Chemistry 2015

We believe that at high temperatures ($\geq$750 °C) decomposition of NH_3 produces reducing species (*e.g.* N_2H_4, H_2) in high abundance relative to reactions at low temperature. The reduction of In_2O_3 into indium is then highly favoured. The resulting indium metal particles embedded or supported on the 3D particle or the 2D sheet, could serve as catalysts from which indium filled InN nanotubes grow. This is supported by experiments we performed by conventional thermal nitridation of In_2O_3 (not shown), where at high temperatures all the In_2O_3 is converted to metallic indium. Thus UV irradiation aids in activating the nitriding species at lower temperatures to limit complete conversion to indium metal.

3 Experimental

In_2O_3 powder (Aldrich, particle size 300–600 nm, 99.99% purity) was placed in a quartz boat (*L*: 25 mm, *D*: 8 mm) that had been cleaned in ethanol. The boat was then loaded into a long quartz tube (*L*: 800 mm, *D*: 20 mm) which was installed horizontally into a furnace. The furnace has an opening (*D*: 30 mm) that allowed light from a mercury UV lamp in to the mid-region of the furnace to illuminate the tube and its contents. A 400 Watt medium pressure mercury UV lamp (model no. 3040, Photochemical reactors Ltd) was situated in a housing equipped with a cooling system (Fig. 1).

The quartz tube was degassed and purged with high-purity (99.999%) nitrogen. During the growth process, 400 sccm of NH_3 (anhydrous, 99.999%) was introduced into the tube. The flow rate of NH_3 was programmed and maintained at 400 sccm using a Brookes mass flow controller at atmospheric pressure. The exhaust NH_3 was bubbled through an oil bubbler before being discharged into the atmosphere. The furnace was set to 700–800 °C (the temperature error, ± 2 °C) and was held there for 1–6 h, then cooled to room temperature under NH_3.

Two sets of synthesis experiments were carried out. In the first setup (position 1), In_2O_3 powder was not irradiated by the UV lamp to prevent secondary photolysis of the product (Fig. 1) while varying temperature. In the second setup (position 2), both reactants (In_2O_3 and NH_3) were irradiated while varying the synthesis temperature and time (1–4 h). The breakdown of all the reactions and the reaction parameters varied is tabulated in Table S1 (ESI†). A fluffy wool-like grey product was generated at the surface of the quartz boat after nitriding the reactant. In a typical optimised experiment 0.2 g of In_2O_3 was used and 0.08 g of partially filled InN nanotubes was obtained. XRD data used for structural analysis was collected on a Bruker D2 diffractometer with CuKα radiation. Morphologies were evaluated by SEM (NOVA) and TEM (Tecnai T12). The optical properties of InN nanotubes were characterized by diffuse reflectance spectroscopy (Praying Mantis DRS Cary 500) and Raman spectroscopy (Jobin Yvon LabRAM).

4 Conclusions

In this study we have indicated the use of a combined thermal/UV photolysed approach to make InN materials with a wide range of shapes. Photolysis of the NH_3 provides a method to activate the NH_3 that in the presence of In_2O_3 replaces the O atoms by N atoms (a reduction reaction). In doing so the In_2O_3 structure converts from a 3D structure to a 1D tubular material. Secondary growth processes lead to the final structures observed. The InN material that makes the tubes does so by means of supersaturation and nucleation from the catalytic liquid indium metal phase *via* a VLS mechanism. The anisotropic alignment of the indium filled InN nanotubes seen in all SEM images is a typical feature of the VLS method. The rod-like structures made of cones as well as flaky rods could be formed by a VS mechanism.

Photolysis of the In_2O_3 (as well as the NH_3) results in the formation of completely different structures. In this case the replacement of the O in the In_2O_3 by N is aided by the photolysis process. Thus, the solid particles become porous on photolysis as the replacement reaction of O by N progresses (700 °C). With an increase in temperature (800 °C), a pure InN is formed as more indium filled InN tubes are formed. However, over-reduction occurs and indium metal now readily forms.

This study indicates the rich range of InN materials that is accessible by simple synthetic strategies. The study also indicates that the various structures are all linked together *i.e.* the structures form from each other. More work will be required to gain further insight into these shape/size transformation reactions. Whether the methodology can be extended to the synthesis of other metal nitride materials will need further experimentation.

Acknowledgements

References

1 J. B. MacChesney, *Mater. Res. Bull.*, 1970, **5**, 783.
2 S. Vaddiraju, A. Mohite, A. Chin, M. Meyyappan, G. Sumanasekera, B. W. Alphenaar and M. K. Sunkara, *Nano Lett.*, 2005, **5**, 1625.
3 T. J. Kistenmacher and W. A. Bryden, *Appl. Phys. Lett.*, 1991, **59**, 1844.
4 Y. Xia, P. Yang, Y. Sun, Y. Wu, B. Mayers, B. Gates, Y. Yin, F. Kim and H. Yan, *Adv. Mater.*, 2003, **15**, 353.
5 C. N. R. Rao, F. L. Deepak, G. Gundiah and A. Govindaraj, *Prog. Solid State Chem.*, 2003, **31**, 5.
6 M.-S. Hu, W.-M. Wang, T. T. Chen, L.-S. Hong, C.-W. Chen, C.-C. Chen, Y.-F. Chen, K.-H. Chen and L.-C. Chen, *Adv. Funct. Mater.*, 2006, **16**, 537.
7 H. Xu, Z. Liu, X. Zhang and S. Hark, *Appl. Phys. Lett.*, 2007, **90**, 113105.
8 J. Zhang, L. Zhang, X. Peng and X. Wang, *J. Mater. Chem.*, 2002, **12**, 802.
9 T. Tang, S. Han, W. Jin, X. Liu, C. Li, D. Zhang, C. Zhou, B. Chen, J. Han and M. Meyyapan, *J. Mater. Res.*, 2004, **19**, 424.

This journal is © The Royal Society of Chemistry 2015

J. Mater. Chem. A, 2015, **3**, 5962–5970 | **5969**

10 S. Luo, W. Zhou, W. Wang, Z. Zhang, L. Liu, X. Dou, J. Wang, X. Zhao, D. Liu and Y. Gao, *Appl. Phys. Lett.*, 2005, **87**, 063109.

11 B. Schwenzer, L. Loeffler, R. Seshadri, S. Keller, F. F. Lange, S. P. DenBaars and U. K. Mishra, *J. Mater. Chem.*, 2004, **14**, 637.

12 W. Jung, C. S. Ra and B. Min, *Bull. Korean Chem. Soc.*, 2005, **26**, 1354.

13 X. M. Cai, F. Ye, S. Y. Jing, D. P. Zhang, P. Fan and E. Q. Xie, *Appl. Surf. Sci.*, 2008, **255**, 2153.

14 L. W. Yin, Y. Bando, D. Golberg and M. S. Li, *Adv. Mater.*, 2004, **16**, 1833.

15 S. Z. Karazhanov, P. Ravindran, P. Vajeeston, A. Ulyashin, T. Finstad and H. Fjellvåg, *Phys. Rev. B: Condens. Matter Mater. Phys.*, 2007, **76**, 075129.

16 R. Weiher and R. Ley, *J. Appl. Phys.*, 1966, **37**, 299.

17 L. Gao, Q. Zhang and J. Li, *J. Mater. Chem.*, 2003, **13**, 154.

18 S. Luo, W. Zhou, Z. Zhang, L. Liu, X. Dou, J. Wang, X. Zhao, D. Liu, Y. Gao and L. Song, *Small*, 2005, **1**, 1004.

19 S. Luo, W. Zhou, Z. Zhang, X. Dou, L. Liu, X. Zhao, D. Liu, L. Song, Y. Xiang and J. Zhou, *Chem. Phys. Lett.*, 2005, **411**, 361.

20 Y. Hirota and O. Mikami, *Electron. Lett.*, 1985, **21**, 77.

21 D. Ehrlich, R. Osgood Jr and T. Deutsch, *J. Vac. Sci. Technol.*, 1982, **21**, 23.

22 V. Donnelly, M. Geva, J. Long and R. Karlicek, *Appl. Phys. Lett.*, 1984, **44**, 951.

23 H. Ando, H. Inuzuka, M. Konagai and K. Takahashi, *J. Appl. Phys.*, 1985, **58**, 802.

24 G. J. Kavarnos and N. J. Turro, *Chem. Rev.*, 1986, **86**, 401.

25 B. Gellert and U. Kogelschatz, *Appl. Phys. B*, 1991, **52**, 14.

26 D. Ehrlich and R. Osgood Jr, *Thin Solid Films*, 1982, **90**, 287.

27 D. Yu, X. Sun, C. Lee, I. Bello, S. Lee, H. Gu, K. Leung, G. Zhou, Z. Dong and Z. Zhang, *Appl. Phys. Lett.*, 1998, **72**, 1966.

28 W. Shi, Y. Zheng, N. Wang, C. Lee and S. Lee, *Chem. Phys. Lett.*, 2001, **345**, 377.

29 X. Duan and C. M. Lieber, *J. Am. Chem. Soc.*, 2000, **122**, 188.

30 Y.-K. Chang and F. C.-N. Hong, *Mater. Lett.*, 2009, **63**, 1855.

31 L.-W. Yin, Y. Bando, Y.-C. Zhu, D. Golberg and M.-S. Li, *Appl. Phys. Lett.*, 2004, **84**, 3912.

32 X. Wang, S.-B. Che, Y. Ishitani and A. Yoshikawa, *Appl. Phys. Lett.*, 2006, **89**, 171907.

33 V. Y. Davydov and A. Klochikhin, *Semiconductors*, 2004, **38**, 861.

34 K. Butcher and T. Tansley, *Superlattices Microstruct.*, 2005, **38**, 1.

35 A. E. Morales, E. S. Mora and U. Pal, *Rev. Mex. Fis. S*, 2007, **53**, 18.

36 K. Scott, A. Butcher, M. Wintrebert-Fouquet, P. P. T. Chen, K. E. Prince, H. Timmers, S. K. Shrestha, T. V. Shubina, S. V. Ivanov and R. Wuhrer, *Phys. Status Solidi C*, 2005, **2**, 2263.

37 H. Timmers, S. K. Shrestha and A. P. Byrne, *J. Cryst. Growth*, 2004, **269**, 50.

38 M. Yoshimoto, H. Yamamoto, W. Huang, H. Harima, J. Saraie, A. Chayahara and Y. Horino, *Appl. Phys. Lett.*, 2003, **83**, 3480.

39 T. Matsuoka, H. Okamoto, M. Nakao, H. Harima and E. Kurimoto, *Appl. Phys. Lett.*, 2002, **81**, 1246.

40 W. Walukiewicz, S. Li, J. Wu, K. Yu, J. Ager Iii, E. Haller, H. Lu and W. J. Schaff, *J. Cryst. Growth*, 2004, **269**, 119.

41 Y. Ding, P. X. Gao and Z. L. Wang, *J. Am. Chem. Soc.*, 2004, **126**, 2066.

42 E. P. Bakkers and M. A. Verheijen, *J. Am. Chem. Soc.*, 2003, **125**, 3440.

43 L. W. Yin, Y. Bando, J. H. Zhan, M. S. Li and D. Golberg, *Adv. Mater.*, 2005, **17**, 1972.

44 H.-D. Yu, M. D. Regulacio, E. Ye and M.-Y. Han, *Chem. Soc. Rev.*, 2013, **42**, 6006.

45 H.-D. Yu, Z.-Y. Zhang, K. Y. Win, J. Chan, S. H. Teoh and M.-Y. Han, *Chem. Commun.*, 2010, **46**, 6578.

46 H. Yu, D. Wang and M.-Y. Han, *J. Am. Chem. Soc.*, 2007, **129**, 2333.

47 Z. Chen, Y. Li, J. Jiang, C. Cao, T. Xu, Q. Chen, X. Xu and H. Zhu, *RSC Adv.*, 2012, **2**, 6806.

48 V. D. Ashok, T. Ghoshal and S. De, *J. Phys. Chem. C*, 2009, **113**, 10967.

49 J. A. Kaye and D. F. Strobel, *Icarus*, 1983, **54**, 417.

50 E. O. Wiig and G. B. Kistiakowsky, *J. Am. Chem. Soc.*, 1932, **54**, 1806.

51 N. Dietz, M. Straßburg and V. Woods, *J. Vac. Sci. Technol., A*, 2005, **23**, 1221.

52 D. Dirtu, L. Odochian, A. Pui and I. Humelnicu, *Cent. Eur. J. Chem.*, 2006, **4**, 666.

53 J. C. Elgin and H. S. Taylor, *J. Am. Chem. Soc.*, 1929, **51**, 2059.

54 R. R. Wenner and A. O. Beckman, *J. Am. Chem. Soc.*, 1932, **54**, 2787.

5970 | *J. Mater. Chem. A*, 2015, **3**, 5962–5970

This journal is © The Royal Society of Chemistry 2015